Detecting Neutrinos from AGN: New Fluxes and Cross Sections

Gary C. Hill

Department of Physics and Mathematical Physics
University of Adelaide
Adelaide 5005
South Australia
e-mail: ghill@physics.adelaide.edu.au

Abstract

New information on the structure of the nucleon from the HERA *ep* collider leads to higher neutrino cross sections for the processes $\nu_\mu(\bar{\nu}_\mu) + N \to \mu^-(\mu^+) + X$ needed to calculate the expected rates of astrophysical neutrino induced muons in large detectors either under construction, or in the design stage. These higher cross sections lead to higher muon rates for arrival angles where neutrino attenuation in the earth is less important. On the other hand, new estimates of AGN neutrino fluxes suggest that the expected muon rates in these detectors may be much lower than previously calculated. I use the new cross sections to calculate the expected muon rates and angular distributions in large detectors for a variety of AGN models and compare these rates with the atmospheric neutrino backrounds (from both conventional decay channels and the 'prompt' charmed meson decay channels). If the lowest flux estimates are correct, there may be diffculties in determining the origin of a small excess of muons, due to the large uncertainty in the rate of the charmed meson neutrino production channel. However, the more optimistic AGN neutrino fluxes should be detectable in proposed detectors, such as DUMAND-II, AMANDA, NESTOR and Lake Baikal.

Preprint submitted to Astroparticle Physics *1 February 2008*

1 Introduction

In this paper I consider the problem of detecting neutrinos from active galactic nuclei (AGN). Recent predictions (see for example [1,2,3,4,5]) of the diffuse background of neutrinos from the sum of all AGN are high enough that water and ice Cerenkov detectors under construction such as DUMAND [6], AMANDA [7], Lake Baikal [8] and NESTOR [9] should be sensitive to muons from the interactions of the neutrinos in the earth [10,11,12,13,14,15,16]. Most recently, Protheroe [17] has used a new model to calculate the rate of gamma ray and neutrino production in AGN jets. The resulting diffuse neutrino background varies over many orders of magnitude depending upon assumptions made about the relative contributions of various production mechanisms in the AGN system. The minimum estimated flux may be beyond the reach of the current generation of neutrino detectors mentioned above. I have reassessed the detectability of a wide range of flux predictions using calculations of the neutrino cross sections based on nucleon structure function parameterizations [18,19] (parton distributions) derived from recent accelerator experiments [20,21,22,23]. Use of the new parton distributions leads to higher cross sections and a corresponding increased probability of a detectable muon being produced in the rock surrounding a detector. However, increased neutrino absorption in the earth is an important effect and offsets some of the gains for the longest neutrino paths through the earth. I present the rates and angular distributions of muons for different AGN spectra and for the flux of atmospheric neutrinos [24] produced when cosmic rays interact with the earth's atmosphere, including neutrinos from charmed meson decay [13,14,25].

The outline of the paper is as follows. A brief review of the quark parton model and how it is used to calculate neutrino cross sections using accelerator structure function data (parton distributions) is presented. I then examine two of the most recent sets of parton distributions and look at the implications for the total cross sections. Finally, I discuss the use of these cross sections to estimate the rates and angular distributions of neutrino induced muons in large detectors, using a Monte Carlo simulation of the passage of neutrinos through the earth. This has the advantage of allowing a precise treatment of the effects of neutral current scattering, which reduces the neutrino energies before they finally interact to produce muons. The prospects for detection of the AGN fluxes above the atmospheric backgrounds are then examined.

Upon completion of these calculations, I learned of similar work by Gandhi, Quigg, Reno and Sarcevic [16], using another recent set of parton distributions [26], which yield muon rates consistent with the results presented in this work.

2 Quark-parton model and the neutrino cross sections

2.1 Parton model description of charged and neutral current neutrino cross sections

The interaction of a neutrino with a nucleon may be described [27,28] in terms of the quark-parton model. The nucleon is considered to be a collection of quasi-free "partons" (quarks and gluons) which share the nucleon momentum. A proton consists of three valence quarks (up, up and down) surrounded by a sea of quark/antiquark pairs of all flavours. The description of a weak interaction of a neutrino (energy E_ν) with a nucleon (mass M_N) in the quark-parton model is described in terms of an interaction of the neutrino with any one of the individual quarks (which carries a fraction x of the nucleon momentum). In a charged current process a W boson is exchanged from a muon-neutrino to the quark with the neutrino turning into a muon (energy E_μ). A neutral current process involves the exchange of a Z boson, with the neutrino remaining a neutrino. The square of the 4-momentum transfer is denoted Q^2 and the variable $y = \nu/E_\nu$ ($\nu = E_\nu - E_\mu$) describes the fractional energy transfer. The cross section for the inclusive processes $\nu_\mu(\bar{\nu}_\mu) + N \rightarrow \mu^-(\mu^+) + X$ and $\nu_\mu(\bar{\nu}_\mu) + N \rightarrow \nu_\mu(\bar{\nu}_\mu) + X$ can be written in terms of the variables x and $y = \nu/E_\nu$ (referred to as Bjorken scaling variables) where x,y and Q^2 are related to the square of the centre of mass energy $s = 2M_N E_\nu$, by $Q^2 = sxy$.

The cross section for the *charged current* interaction $\nu_\mu(\bar{\nu}_\mu) + N \rightarrow \mu^-(\mu^+) + X$ is written in terms of three structure functions $F_1^{\nu N,\bar{\nu}N}, F_2^{\nu N,\bar{\nu}N}$ and $F_3^{\nu N,\bar{\nu}N}$, but if the transverse momentum carried by the quarks in the nucleon is negligible then the relation $2xF_1 = F_2$ [29] reduces this dependence to two structure functions [30]:

$$\left(\frac{d^2\sigma}{dxdy}\right)^{\nu N,\bar{\nu}N} = \frac{G_F^2 M_N E_{\nu\bar{\nu}}}{\pi}\left[\frac{M_W^2}{Q^2 + M_W^2}\right]^2 \times \left\{(1 - y + \frac{y^2}{2})F_2^{\nu N,\bar{\nu}N}(x,Q^2) \pm (y - \frac{y^2}{2})xF_3^{\nu N,\bar{\nu}N}(x,Q^2)\right\} \quad (1)$$

The $\pm$ sign corresponds to the $\nu/\bar{\nu}$ cross sections. M_W is the mass of the W-boson and $G_F (= 1.16639 \times 10^{-5}\ \mathrm{GeV}^{-2})$ is the Fermi constant [31]. The cross section in equation 1 is expressed in natural units where $\hbar = c = 1$ yielding a result in units of GeV^{-2}, to convert to a cross section in cm^2 we multiply by $0.38939 \times 10^{-27}\ \mathrm{cm}^2\ \mathrm{GeV}^2$ [28]. Equation 1 also holds for $\nu_e(\bar{\nu}_e) \rightarrow e^+(e^-)$.

The structure functions F_2 and F_3 are defined in terms of quark distri-

butions [32]:

$$F_2^{\nu N,\bar{\nu}N} = x(q + \bar{q}) \tag{2}$$

and

$$F_3^{\nu N,\bar{\nu}N} = q - \bar{q} \pm 2\{[s - c] + [b - t]\} \tag{3}$$

where

$$\begin{aligned} q &= u + d + s + c + b + t \\ \bar{q} &= \bar{u} + \bar{d} + \bar{s} + \bar{c} + \bar{b} + \bar{t} \end{aligned} \tag{4}$$

are the sums of the quark/antiquark distributions (u, d, s, etc). Each quark distribution is a function of x and Q^2 describing the number of quarks of that flavour having a fractional momentum in the range $x \rightarrow x + dx$, at momentum scale Q^2. Note that the $\pm$ sign again corresponds to the $\nu/\bar{\nu}$ cross sections.

The *neutral current* cross sections $\nu_\mu(\bar{\nu}_\mu) + N \rightarrow \nu_\mu(\bar{\nu}_\mu) + X$ are expressed in the same form as equation 1, but with M_W replaced by M_Z and the structure functions F_2 and F_3 written as [33]

$$\begin{aligned} F_2 = {} & x(q + \bar{q})[\delta_1^2 + \delta_2^2 + \delta_3^2 + \delta_4^2] \\ & + 2x[(c - s) + (t - b)][\delta_1^2 + \delta_3^2 - \delta_2^2 - \delta_4^2] \end{aligned} \tag{5}$$

and

$$F_3 = (q - \bar{q})[\delta_1^2 + \delta_2^2 - \delta_3^2 - \delta_4^2] \tag{6}$$

The δ factors are the chiral couplings, defined in terms of the weak mixing parameter $x_W = \sin^2\theta = 0.225$ [31]

$$\begin{aligned} \delta_1 &= \frac{1}{2} - \frac{2}{3}x_W \\ \delta_2 &= -\frac{1}{2} + \frac{1}{3}x_W \\ \delta_3 &= -\frac{2}{3}x_W \\ \delta_4 &= \frac{1}{3}x_W \end{aligned} \tag{7}$$

2.2 Parton distributions derived from recent accelerator data

For this work the cross sections have been calculated using sets of parton distributions [18,19] fitted to the latest HERA deep inelastic scattering data [20,21,22,23]. The H1 and ZEUS collaborations have extracted the electromagnetic structure function F_2^{ep} from collisions of 26.7 GeV electrons with 820 GeV protons. F_2^{ep} is the sum of the individual parton distributions weighted by the squares of their electric charges :

$$F_2^{ep} = \frac{4}{9}(u + \bar{u}) + \frac{1}{9}(d + \bar{d}) + \frac{4}{9}(c + \bar{c}) + \frac{1}{9}(s + \bar{s}) + \frac{1}{9}(b + \bar{b}) \tag{8}$$

From the F_2^{ep} measurement the individual quark distributions can be calculated and used to form the structure functions $F_2^{\nu N}$ and F_3 needed for the neutrino nucleon cross section calculation. However, to calculate the cross section in the energy range $10^5 - 10^8$ GeV, we need to know the parton distributions at higher Q^2 than the HERA measurements. QCD theory [37,38,39,40] describes the evolution of the parton distributions to higher Q^2. I consider two different solutions of the evolution equations, which predict sufficiently different behaviour in the unknown regions of Q^2 and x to give neutrino cross sections up to a factor of two bigger than previous calculations [34,35,36] in the energy range of interest. Martin, Roberts and Stirling have presented several sets of parton distributions [41,42,43] based on the increasing amount of accelerator data. Their latest parton set ("MRS G") [18] is a parameterisation that includes the recent HERA F_2 data. The MRS fits supply individual parton distributions $u_v, d_v, u_s, d_s, s_s, c_s, b_s$ which can be used to form F_2 and F_3.

In their recent work [19] Frichter, McKay and Ralston have effectively fitted a two parameter (A, μ) solution of the structure function evolution equations to the HERA F_2^{ep} data :

$$F_2^{ep}(x, Q^2) = Ax^{-\mu} \frac{P_{qg}(1+\mu, Q^2)}{P_{gg}(1+\mu, Q^2)} \times \exp\left\{ \ln\ln\left(\frac{Q^2}{\Lambda^2}\right) \ln\left(\frac{Q^2}{\Lambda^2}\right) P_{gg}(1+\mu, Q^2) \right\} \tag{9}$$

Λ is the QCD scale parameter (taken as $200MeV$ in the FMR result) and $P_{qg}(1+\mu, Q^2)$ and $P_{gg}(1+\mu, Q^2)$ are the $1+\mu$ moments of the quark-gluon and gluon-gluon splitting functions, evaluated at next to leading order [33,44,45]. In order to obtain $F_2^{\nu N}$, FMR make the assumption that the quark (q_i) and anti-quark $(\bar{q}_i)$ distributions of the ith flavour are equal, and that

$$q_i = \bar{q}_i = u = d = s = 2c = 2b \tag{10}$$

Substituting into F_2^{ep} and $F_2^{\nu N}$ yields $F_2^{ep} = \frac{17}{9} q_i(x, Q^2)$ and $F_2^{\nu N} = 8 q_i(x, Q^2)$ from which we obtain :

$$F_2^{\nu N} = \frac{72}{17} F_2^{ep} \tag{11}$$

A least squares minimization to the 1992 and 1993 HERA F_2^{ep} data yields best fit parameters $A = 0.008829$ and $\mu = 0.3856$.

2.3 The total neutrino charged and neutral current cross sections

To obtain the total cross sections I have integrated equation 1 using the MRS G and FMR parton distributions, for both the charged and neutral current forms of F_2 and F_3.

The MRS G distributions cover the full range $0 < x < 1$ required, but the FMR result applies only at $x \sim 0.2$ or less. In order to evaluate the FMR cross section over the full x range, I have used the FMR result for $x < 0.2$ and the MRS G result for $x \geq 0.2$. The MRS G parton distributions are valid down to $x \sim 10^{-5}$, which is adequate for the calculation of the cross sections in the energy range considered in this work ($E_\nu < 10^8$ GeV). (Note that the double-logarithmic approximation [46] may be used to extrapolate the parton distributions to lower x for cross section calculations [34,35,36] where $E_\nu > 10^8$GeV.)

Note also that I have combined a set of *next-to-leading order* (NLO) parton distributions (MRS G) calculated in the $\overline{MS}$ renormalization convention with the *leading order* (LO) form of the structure functions F_2 and F_3. The NLO expressions for F_2 and F_3 (obtained by convolving the quark and gluon distributions with the Wilson coefficients [47]) will differ from the LO expressions by terms with coefficients $\alpha_S(Q^2)/2\pi$, where $\alpha_S(Q^2)$ is the QCD coupling constant, which decreases as Q^2 increases. In the regions of high Q^2 ($\sim M_W^2$) important for the neutrino energies considered in this work $\alpha_S(Q^2)/2\pi$ has a value of ~ 0.02 and the resulting differences between the LO and NLO structure functions, and hence the difference in the resulting cross sections, will be small ($\sim$ a few percent). Given the very large uncertainties in the astrophysical assumptions in this work, this is an acceptable approximation.

The total neutrino/anti-neutrino charged/neutral current cross sections obtained by using the FMR and MRS G parton distributions are shown in figure 1, along with the "$B-$ " neutrino charged current estimate by Reno [36]. Above 10^5 GeV neutrino and anti-neutrino cross sections are equal and the FMR cross sections are roughly 1.5 times bigger than the MRS G predictions and 2 times bigger than the Reno $B-$ prediction. The recent calculations of

Gandhi *et al* [16], using the CTEQ3 parton distributions [26], yield a neutrino charged current cross section lower than using MRS G by about 7% at 10^3 GeV, with difference rising to 23% at 10^8 GeV. The CTEQ3 cross section is bigger than the Reno $B-$ cross section by 1-10% in the same energy range.

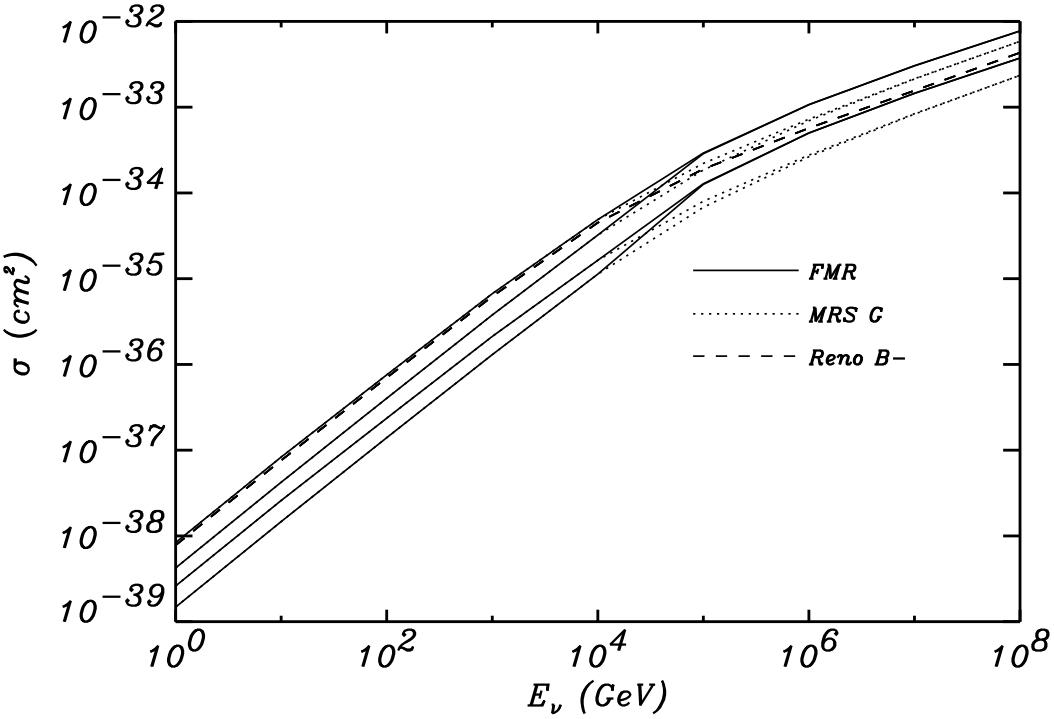

Fig. 1. Total ν and $\bar{\nu}$ cross sections calculated using recent parton distributions. At low energy the curves represent (in decreasing order of cross section) ν - charged current, $\bar{\nu}$ - charged current, ν - neutral current and $\bar{\nu}$ - neutral current. At high energy, neutrino and anti-neutrino cross sections are equal.

3 Astrophysical neutrino fluxes

The reported observations [48,49,50,51] of UHE γ–rays from binary X-ray systems in the early 1980s led to predictions of neutrino fluxes from such objects. The assumption was that protons accelerated in the vicinity of the compact object would interact with other matter in the system to give both neutral and charged pions, the neutral pions decaying to produce the observed γ–rays and the charged pions producing a neutrino flux. Calculations were made [30,34,52,53,54] of the expected neutrino flux by scaling the models to the observed γ–ray flux. However the non-confirmation of the γ–ray observations by much larger and more sensitive air shower arrays such as CASA [55,56,57,58,59] has led to upper limits on the γ–ray fluxes that are orders of magnitude lower than the original detection claims, dampening expectation of observable neutrino fluxes from binary X-ray systems.

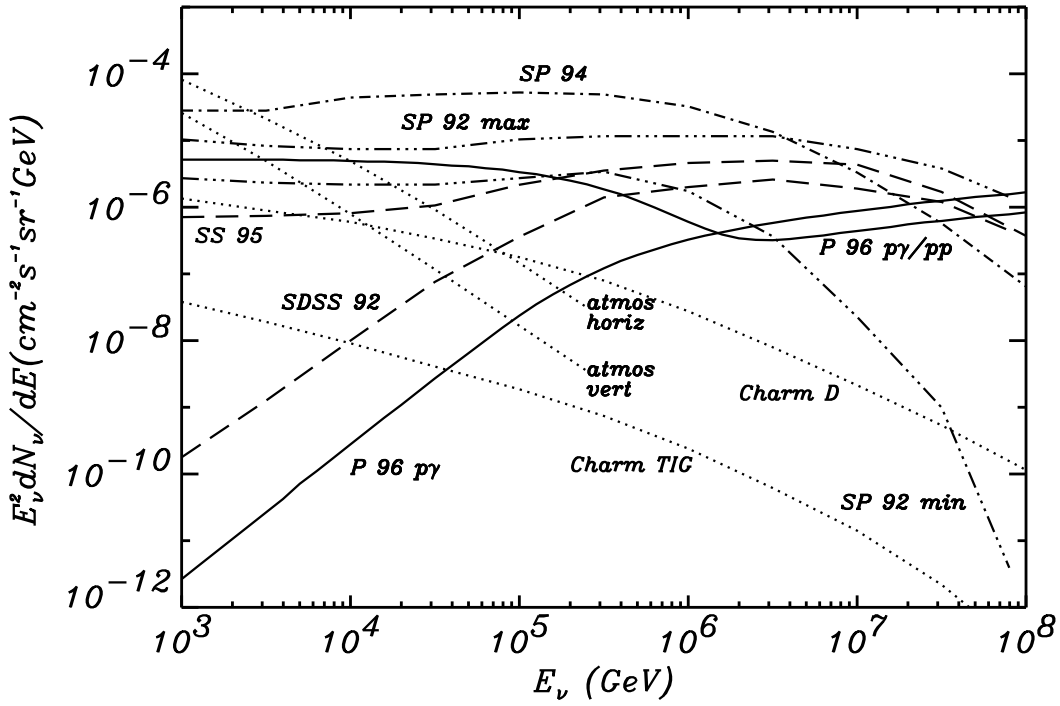

Fig. 2. Diffuse isotropic neutrino fluxes from the sum of all active galactic nuclei predicted by various models. The angle dependent neutrino flux produced from cosmic ray interactions in the earth's atmosphere is also shown for horizontal and vertical directions. The isotropic neutrino flux produced from prompt decays of charmed mesons in the atmosphere is also shown.

Attention in recent times has focussed on the production of neutrinos in active galactic nuclei, where particle acceleration may be occuring at accretion shocks in the vicinity of massive black holes. Stecker, Done, Salamon and Sommers (SDSS) [1,2] calculated the neutrino flux resulting from interactions of protons with energy above the threshold energy for photoproduction on UV photons ($p\gamma \rightarrow \Delta \rightarrow n\pi^+$). Szabo and Protheroe (SP) [4,5] included all the subsequent interactions of the protons after the initial photoproduction. Luminosity functions [60,61] (derived from X-ray and gamma-ray measurements - describing the luminosity of AGN as a function of redshift) and the relationship between the neutrino and X-ray and gamma-ray outputs in a given AGN model were used to calculate the neutrino output from the sum of all AGN in the universe. More recently Stecker and Salamon [3] revised their original model and calculated diffuse neutrino backgrounds for quasar cores and blazar jets.

Protheroe [17] has calculated the neutrino and gamma-ray fluxes from proton acceleration in 'blobs ' of matter in AGN jets. Two major production mechanisms were considered. Accelerated protons may leave the blob and interact with the radiation field of the accretion disk ($p\gamma$ interactions), or interact with each other or with other matter in the vicinity (pp interactions).

The observed time variability of gamma-rays from AGN such as MKR421 place constraints on the relative contribution of each mechanism. The pp interactions have a long characteristic time scale and therefore cannot produce variability of the order of a day. The $p\gamma$ contribution, however, can vary rapidly and must be responsible for the time variation. To produce an intensity change of a factor of 2 over a short time scale, the pp interaction can contribute no more than about 50% to the total output. The pp interactions produce the most neutrinos, so the maximum allowable neutrino flux comes from equal contributions of pp and $p\gamma$ and the minimum flux from 100% $p\gamma$. The luminosity function [62] derived from the EGRET survey and the results from the SAS-2 experiment [63] have been used to produce a diffuse neutrino background estimate.

Figure 2 shows the resulting neutrino fluxes from a number of different models. Note that the fluxes are multiplied by E^2 to reduce the range of the plot. Curves labelled 'SP' (dot-dashed lines) are predictions from the earlier Szabo and Protheroe models. 'SDSS92 ' is the Stecker *et al* $p\gamma$ flux, while 'SS95' is the sum of the quasar core and blazar jet contributions in the Stecker and Salamon model (dashed lines). The new Protheroe model is shown in solid lines for the limiting cases, the minimum expectation coming from $p\gamma$ interactions only and the maximum from equal contributions from pp and $p\gamma$ interactions.

The major backgrounds to searches for AGN fluxes come from the decay of kaons, pions and muons produced from the interactions of cosmic rays in the earth's atmosphere. These fluxes show an angular dependence; in the horizontal direction the fluxes at the surface are greatest as the kaons, pions and muons traverse more atmosphere and have more time to decay. The results of Lipari [24] are shown. Another potential background comes from the prompt decay of charmed particles produced in cosmic ray interactions in the atmosphere. The expected neutrino fluxes should have a flatter energy spectrum and not show an angular dependence as the particles mostly decay before they can interact. Zas, Halzen and Vázquez [13] have calculated the expected neutrino fluxes from charmed meson decay under various assumptions of the charm production cross section and have computed muon rates in downward looking detectors. Gaisser, Halzen and Stanev [14] conclude that model B is an upper limit to the neutrino fluxes in the region $E_\nu > 100$ TeV. However, model D predicts higher fluxes at lower neutrino energies and gives overall the highest muon rates in downward looking detectors of the two cases. I therefore use model D to predict the upper limit on the muon rate from charm production. As a lower limit, I take the prediction of Thunman, Ingelman and Gondolo [25] which gives neutrino fluxes nearly 100 times smaller than the ZHV model D. It is clear that there is a large uncertainty in the potential contribution of charmed meson decay to the neutrino induced muon fluxes. The implications of this on the detectability of the AGN fluxes will be addressed in the next section.

4 Neutrino induced muon rates in large detectors

4.1 The neutrino interaction Monte Carlo

Cerenkov detectors (DUMAND, AMANDA, NESTOR, Lake Baikal) detect upward going muons from charged current interactions of neutrinos in the earth. The muons can be produced many kilometres from the detector and still survive to be detected via their Cerenkov emissions in water or ice. Calculations of the expected muon fluxes from AGN [10,11,12,13,14] have been made using various parton distributions and muon energy loss assumptions. In their original cross section paper [19], Frichter, McKay and Ralston calculated the rates of charged lepton production in a cubic kilometre volume of ice and noted that despite the increased attenuation with their new cross section, the increased interaction probability more than compensated for this, resulting in increased lepton production. In later work [15], they calculated the specific rate expectations for a radio receiver in Antarctic ice, detecting radio Cerenkov radiation from electrons. The highest of the Szabo and Protheroe fluxes [5] and the Stecker *et al* flux [1] were used, the results suggesting these fluxes would be readily detectable with a single antenna buried at a depth of 600 metres. Zas, Halzen and Vázquez [13] calculated the detection rates of neutrino induced horizontal air showers and underground muons, again for SDSS and SP fluxes. These calculations included the expected rates from charm induced neutrinos. The cross sections were calculated with the KMRSB-5 [64] parton distributions which give total cross sections of about the size of the Reno $B-$ estimate. Most recently, Gandhi, Quigg, Reno and Sarcevic [16] (GQRS), have evaluated the cross sections for a variety of parton distributions and have then used the CTEQ3 parton distributions [26] to estimate muon rates from astrophysical sources. Due to the relative differences in the final cross sections, the CTEQ3 partons will yield muon rates closer to those using Reno $B-$ than MRS G.

The calculation of muon fluxes induced by neutrino interactions in the earth is complicated by neutrinos undergoing neutral current interactions in the earth (which reduce their energies but do not remove them from the beam) before they finally interact to produce a muon. The final number of neutrinos in a given energy bin after passage through the earth is reduced by both charged and neutral current interactions, but some of the total loss is offset by originally higher energy neutrinos having moved down in energy due to neutral current interactions.

An effective total cross section can be calculated, which is dependent on the original source spectrum. This approach was followed by Berezinsky *et al* [65] where the total cross section was taken as the sum of neutral and

charged current cross sections, with a correction term included to account for the source dependent neutral current neutrino regeneration effect.

As an alternative approach to the neutral current effect, I have developed a Monte Carlo simulation [66] to model the passage of the neutrinos through the earth, taking into account the relative likelihood of neutral and charged current interactions, and selecting the final neutrino or muon energy from the energy dependent y distributions. A simple weighting system was devised (and generalized to account for neutrinos that undergo none, one, two or more neutral current scatters before a charged current interaction) to keep the computing time reasonable. Neutrinos and anti-neutrinos were treated separately using the appropriate cross sections. The column density of nucleons to be traversed by a neutrino as a function of nadir angle is calculated using the Preliminary Reference Earth Model [67], which describes how the density of the earth varies with distance from the centre. The final energy of a muon reaching the detector is determined using the muon propagation code of Lipari and Stanev [68]. The muon energy losses due to bremsstrahlung [69], e^+e^- pair production [70] and photonuclear interactions [71] are treated stochastically in order to give the correct final fluctuations in muon ranges. Ionization losses are also taken into account. Only muons which are produced within the final tens of kilometres from the detector will actually survive to the detector, so for these calculations I use "standard rock" ($Z = 11, A = 22, \rho = 2.65$ g cm^{-3}) for the propagation.

4.2 Integral neutrino induced muon rates

I have calculated the expected muon rates using the cross sections Reno $B-$, FMR and MRS G resulting from the parton distributions described in section 2.2 which are derived from the latest accelerator structure function data. The higher cross sections result in greater attenuation of neutrinos within the earth, but this effect is offset by a greater probability of muon production by the surviving neutrinos in the final kilometres of rock before a detector, leading to greater expected muon rates. It is important to remember that the effective area of a detector will have an energy and arrival angle dependence and that the overall detection rate will depend upon the energy and angular spectrum of muons incident upon the detector. For example, the effective area for muon detection (averaged over arrival direction) [72] by the DUMAND-II detector (20000m^2 geometric area) varies from about 5000m^2 at 10 GeV (the array does not trigger on all muons) up to 20000m^2 at 5 TeV and goes up to 60000m^2 at 10^7 GeV (the array triggers on muons that pass outside the detector volume). The muon rates calculated here assuming a spherical detector with a constant 20000m^2 effective area for all arrival directions and all muon energies will therefore be approximate lower bounds on the numbers

of muons detected for muons above about 1 TeV (near the energy at which the effective area equals the geometric area). Due to the increase in effective area at higher energies, the muon rates for flatter spectra will be enhanced over those of steeper spectra compared to the numbers presented here which are calculated for an energy independent effective area. Keeping this in mind, we examine the predicted muon rates induced by AGN neutrinos.

The integral muon rates expected in a downward looking detector (2πsr field of view) are shown in figure 3 for the three different cross sections and nine different neutrino spectra of figure 2. The predicted muon fluxes span several orders of magnitude. The SP94 flux exceeds the atmospheric background for a muon energy cut of a few GeV. At the other extreme, the P96pγ does not exceed the atmospheric background until an energy of around 10 TeV. The wide variation in the expected number of muons from charm induced neutrinos is evident. The TIG neutrino flux induces a very low rate of muons, around 1/10 of the lowest AGN flux (P96pγ), and should not pose a background problem at any muon energy cut. However, the ZHV D neutrino flux results in a muon rate exceeding that of the SDDS92 flux for muon energies up to $\sim$400 GeV, and roughly equal to that of the conventional atmospheric and P96pγ fluxes at a muon energy cut of 10 TeV. This great uncertainty suggests that there would be difficulties in identifying the origins of any observed muons should the lowest AGN flux be correct.

The results presented here are not directly comparable to those of Gandhi *et al* [16], as the neutrino source spectra used in both cases are not identical. GQRS made a broken power law approximation to the SP94 (b=1) neutrino flux; this yields muon rates less than the SP94 curve in figure 3, which comes from using the highest of the SP94 fluxes. GQRS also calculated muon rates for the SS95 neutrino flux, but only for the quasar core component, whereas I have used the sum of quasar core and blazar jet components. Also, GQRS treat neutral currents by taking two cross sections: the first the sum of charged and neutral current cross sections, which gives a lower limit to the muon rate; the second the charged current cross section alone, which will give an upper limit to the muon rate. To check the consistency of the two sets of results, I have used the forms of the neutrino fluxes as implemented by GQRS with the MRS G and Reno $B-$ cross sections and find that the muon rates obtained are consistent with the differences in cross sections in the two sets of work.

4.3 Limits from the Fréjus experiment

The SP94 and SP92max fluxes have already been excluded by an analysis of the energy distribution of horizontal neutrino-induced muons in the Fréjus experiment [73,74]. The Fréjus detector was a fine grain tracking calorime-

ter operated deep underground, with the ability to accurately determine the energy of the through going muons from the energy deposited from electromagnetic showering. At near horizontal angles the background atmospheric muon flux is sufficiently suppressed by the rock overburden to allow a measurement of the rate of atmospheric and AGN induced muons. The number of muons (producing an observed energy loss in the detector greater than the maximum observed energy loss) expected from each AGN spectrum has been calculated [14,73,74,75] taking into account the rock thickness, muon propagation and the increasing efficiency of the detector with increasing muon energy. The high fluxes SP94 and SP92max predict more muons than the 90% confidence level upper limit of 2.3 muons and are therefore excluded by this experiment. All the other fluxes considered predict less than 2.3 muons and are therefore not excluded by the Fréjus result.

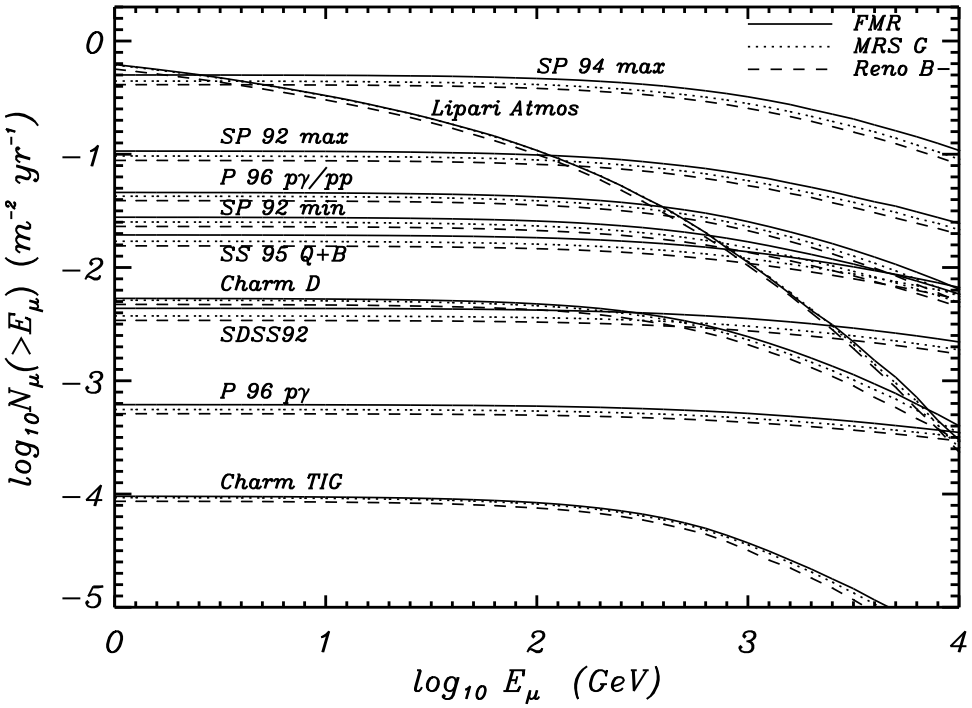

Fig. 3. Integral neutrino-induced muon rates in downward looking detectors as a function of neutrino source spectrum and parton distribution used in the cross section estimate.

4.4 Effects of the higher neutrino cross sections

The angular distributions of the muon fluxes for muon energies above 10^3 GeV and 10^4 GeV are shown in figure 4 for a collecting area of 20000 m^2, which corresponds to that of the proposed nine string DUMAND-II array. The increases in the overall muon rates predicted by the FMR cross section are

not uniform over arrival direction. It is clear that most of the increases come from the highest nadir angles (muons coming from angles 0 to ∼30 degrees down from the horizon) where the thickness of the earth traversed by the neutrinos is smaller and attenuation less important while the likelihood of muon production near the detector is greater. The rate of directly upgoing muons is very similar for all three cross sections considered - the increased rate of muon production in the final kilometres of rock is balanced by increased neutrino attenuation in the earth. The increase in muon rates comes from arrival directions where surface or shallow detectors are most susceptible to noise contamination from downward going atmospheric muons mis-reconstructed as horizontal or upward going. However, deep underwater detectors which are better shielded from atmospheric muons will be sensitive to these increased near horizontal fluxes. For example, the DUMAND-II detector is expected to be sensitive to muons from downgoing neutrinos up to ∼20 degrees above the horizon.

4.5 Detectability of predicted AGN fluxes

Here we consider only those neutrino predictions that have not been ruled out by the Fréjus experiment. The total muons expected for nadir angles greater and less than 60 degrees as a function of muon energy cut and cross section for each neutrino source are summarized in table 1. It is evident that the highest of these fluxes may be observable over the atmospheric background for a 100 GeV muon energy cut (∼300-500 events per year above ∼2000 background) but that the smaller fluxes (10-100 events per year) would not.

For a muon energy cut of 1 TeV, the atmospheric background is significantly reduced and the fluxes P96$p\gamma/pp$, SP92min and SS95 Q+B are now greater than the background and should be observable. The lower SDSS92 flux would produce ∼55-70 events per year above a 225 background and should be observable over several years but an uncertain contribution from charm induced neutrinos (∼1-50 muons) would complicate matters. However figure 4 shows that the charm induced muons have a flat angular distribution and this might aid in identification. The P96$p\gamma$ is well below the background and given the charm uncertainty, would seem not to be detectable.

Moving to a 10 TeV cut reduces the atmospheric background to ∼5 per year, making all the fluxes readily observable, except for the lower bound of P96$p\gamma$. This latter flux, the atmospheric background and the highest charm decay estimate (ZHV D) produce roughly equal numbers of muons. Given that the charm induced muon rate could actually be practically zero (as table 1 shows), this would make a differentiation between charm induced and AGN

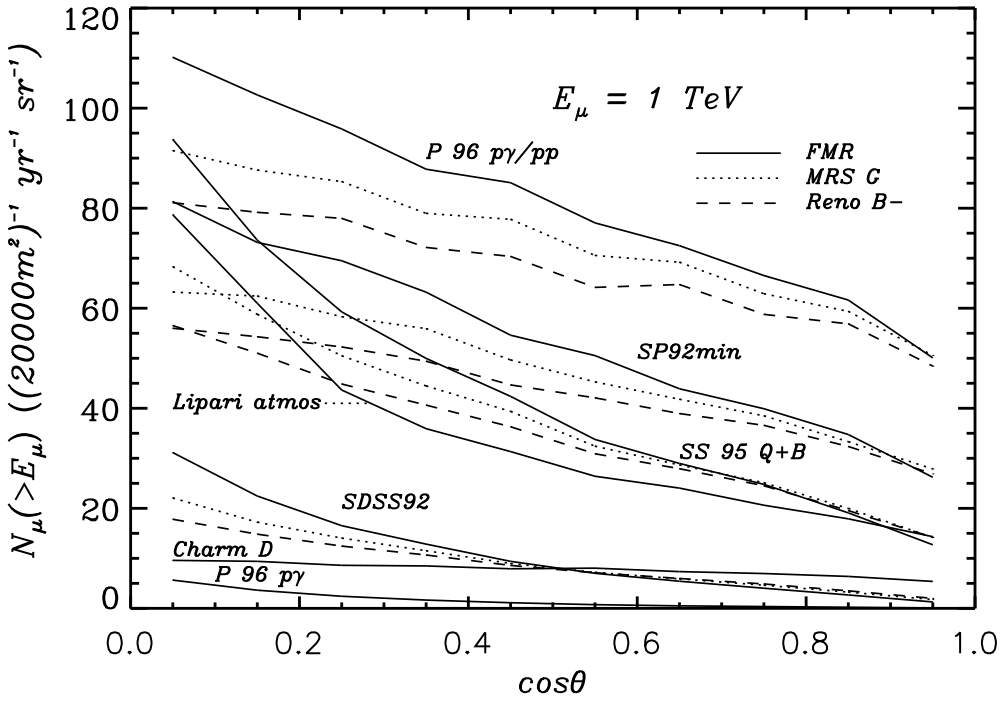

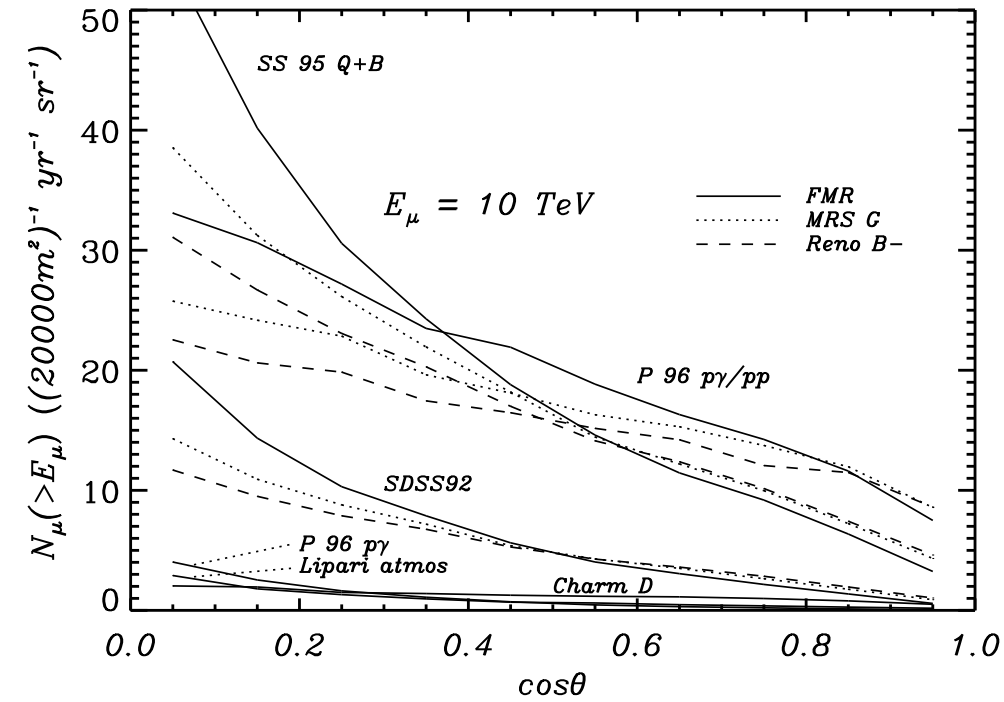

Fig. 4. Muon angular distributions for a 20000m^2 downward looking detector employing a muon energy cuts of 10^3 and 10^4 GeV, for neutrino fluxes not excluded by the Fréjus experiment. For clarity, only the FMR cross section results are shown for the smaller fluxes.

Table 1
Integral muon rates in a 20000m^2 downward looking detector for nadir angles $0-60^o$ (most upgoing) and $60-90^o$ (nearer horizontal) for various neutrino spectra, cross sections and minimum muon energies.

Muon energy cut →		$E_\mu > 10^2$ GeV		$E_\mu > 10^3$ GeV		$E_\mu > 10^4$ GeV	
Nadir angle →		$\theta > 60°$	$\theta < 60°$	$\theta > 60°$	$\theta < 60°$	$\theta > 60°$	$\theta < 60°$
FMR	Atmos	1421	744	157	65	4.8	1.2
	SDSS	68	16	58	13	37	7.0
	SP92min	315	200	215	123	83	34
	SS 95 Q+B	258	109	200	75	105	28
	P 96 pγ/pp	483	358	303	206	86	43
	P 96 pγ	10.5	1.5	9.1	1.2	6.3	0.7
	Charm D	52	43	28	21	5.1	2.9
	Charm TIG	0.9	0.8	0.4	0.3	0.06	0.03
MRS G	Atmos	1394	767	158	67	4.1	1.1
	SDSS	55	17	46	14	29	8.2
	SP92min	272	193	182	117	65	33
	SS 95 Q+B	214	108	164	76	85	30
	P 96 pγ/pp	434	343	265	196	69	41
	P 96 pγ	9.4	1.8	7.9	1.5	5.5	0.9
	Charm D	49	43	25	21	4.2	2.7
	Charm TIG	0.9	0.8	0.4	0.3	0.05	0.03
Reno B-	Atmos	1284	710	145	63	3.6	1.1
	SDSS	48	18	40	15	26	8.6
	SP92min	244	181	161	111	58	32
	SS 95 Q+B	189	105	144	74	74	31
	P 96 pγ/pp	393	320	239	184	61	39
	P 96 pγ	8.0	1.9	7.0	1.6	4.9	1.0
	Charm D	46	39	24	18	3.4	2.4
	Charm TIG	0.8	0.7	0.4	0.3	0.04	0.03

induced muon fluxes difficult, if only a small excess above the expected conventional atmospheric rate was seen. One could not simply do a counting experiment as the excess above the conventional atmospheric background could come from either of two sources. An examination of the angular distributions or differential energy spectra of the detected muons would be needed.

The P96$p\gamma$, Charm D and conventional atmospheric fluxes produce different angular distributions, shown in figure 5. The shape of the atmospheric neutrino induced muon curve reflects primarily the angular distribution of the source neutrinos. The isotropic charm-induced neutrinos produce a flatter angular distribution; but with muons resulting from higher energy neutrinos the angular shape shows evidence of some neutrino absorption. The muons induced by the isotropic P96$p\gamma$ flux show a strong angular dependence due to contributions from much higher neutrino energies. The three angular distributions are quite different for nadir angles greater than 60^o ($\cos\theta < 0.5$). A detector located deep enough such that atmospheric muons are not a problem should be sensitive to these differences, provided enough muons were measured to reveal the angular shape (requiring many years exposure for a 20000 m^2 detector or a much larger detector).

Surface or shallow detectors are affected by misreconstruction of downward muons, which restricts their acceptance aperture. Figure 5 shows that for nadir angles less than 60^o ($\cos\theta > 0.5$) the angular distributions of all three spectra are the same shape (fairly flat). Thus, even using a very large detector/long exposure time but with restricted aperture, the angular distribution alone is not sufficient to determine how much of a small excess of muons was due to AGN, because of the large uncertainty in the charm induced neutrino flux.

Measuring the energy spectrum of the observed muons may allow a differentiation between source spectra. The P96$p\gamma$ and Charm D fluxes give equal numbers of muons above 10 TeV; however $\sim$95% of the Charm D muons are in the energy range 10-100 TeV. The P96$p\gamma$ muons are split roughly equally between the range 10-100 TeV and the region above 100 TeV. A comparison of the excesses in each of these energy regions may aid identification. However, we are dealing with very low count rates where statistical fluctuations and the uncertainty in the conventional atmospheric neutrino flux will also play a role.

As we have just seen, determining the origin of a small excess of muons above the conventional atmospheric expectation relies on looking for angular or energy distribution characteristics. The P96$p\gamma$ and Charm D spectra produce sufficiently different muon distributions to allow them to be distinguished. The integral muon energy spectrum (figure 3) for the P96$p\gamma/pp$ flux is similar to the Charm D muon spectrum, although it produces an absolute level of muons about a factor of 10 bigger. Also the angular distributions for

the P96$p\gamma$/pp flux have near the same slopes as the Charm D angular distributions. This shows that the higher the contribution from pp interactions to the diffuse AGN flux, the more the muon energy and angular distributions become similar to those from the charm induced neutrinos. An AGN spectrum made up of only 10% pp and 90% $p\gamma$ contributions produces a differential muon spectrum with ∼85% of the muons (above 10 TeV) in the energy range 10-100 TeV, and an absolute level only a few times bigger than the Charm D muon spectrum. This shows that a small observed muon excess showing angular and energy distribution characteristics typical of the charm induced muon spectra could actually be due to a combination of an AGN spectrum with a modest pp contribution with a low overall flux level (of order of the P96$p\gamma$ flux given here) and a charm spectrum lower than the Charm D spectrum considered here.

In this discussion I have considered models which produce low numbers of muons in large detectors. Clearly, there will be unambiguous signatures of AGN fluxes if the more optimistic fluxes are correct. Excesses well above those predicted by the Charm D flux will be clear evidence of an extra terrestrial origin. The P96$p\gamma$ flux, although of the same level as the Charm D flux, has distinctive characteristics (flatter muon energy spectrum and steeper angular distribution) that set it apart from the charm induced muons. However, AGN spectra with only modest pp contributions produce muon distributions with similar characteristics to the charm induced muons. Interpreting a small observed excess of muons above the conventional atmospheric expectation will require a better understanding of the production of neutrinos from the prompt decay of charmed particles in the atmosphere.

5 Conclusions

In this work I have calculated the expected AGN neutrino induced muon rates in large detectors and have compared them to the backgrounds expected from atmospheric neutrinos (produced by the decay of pions, kaons, muons and the prompt decay of charmed mesons). A Monte Carlo simulation has been used which correctly accounts for the effects of neutral current scattering and uses cross sections calculated with the FMR and MRS G parton distributions, which were derived from recent accelerator data. These higher cross sections result in greater muon rates due to a greater probability of muon production in the final kilometres before a detector, but for incident neutrino directions in the 120 degree aperture about the nadir this effect is largely offset by increased neutrino absorption. The increases in muon rates come from nadir angles greater than 60 degrees, the region where surface or shallow detectors are most susceptible to atmospheric muon contamination. The very deepest detectors will be able to observe these increased fluxes.

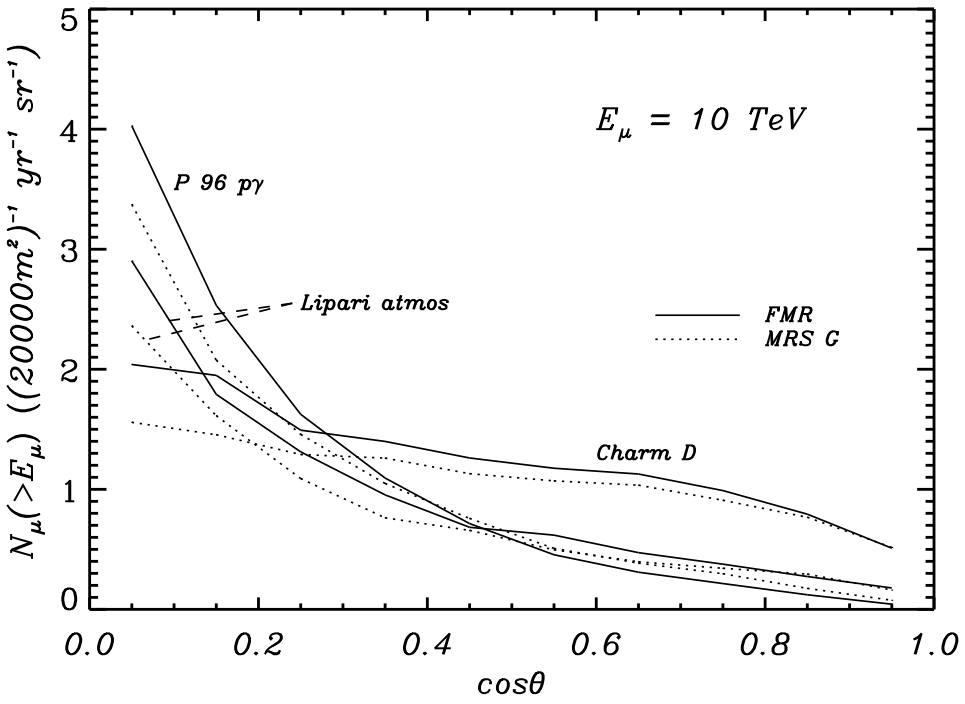

Fig. 5. Muon angular distributions for a 20000m^2 downward looking detector employing a muon energy cut of 10^4 GeV. The curve labelled *Charm D* is an upper estimate of the muons from the prompt decay of charmed mesons into neutrinos in the atmosphere and could be up to two orders of magnitude smaller.

The lowest neutrino flux considered, due to $p\gamma$ interactions only in the Protheroe AGN model, would produce roughly 6 muons per year above 10 TeV in a 20000 m^2 detector, which is about the same as that expected from the conventional atmospheric sources and the same as expected from the highest estimates from charmed meson decay. The lowest neutrino induced muon flux due to charmed meson decay gives practically negligible muon rates, which suggests that telling these sources apart may be difficult. However, the P96$p\gamma$ AGN flux produces muons with angular and energy characteristics that would allow it to be distinguished from the charm and conventional atmospheric backgrounds. On the other hand, an AGN flux with around 10% or more contribution from *pp* interactions produces muon angular and energy distributions similar to those of the charm induced muons. An observation of muons seemingly consistent with the level of the Charm D flux could actually be due to an AGN spectrum with a modest *pp* contribution and an overall flux level around 1/10 th of the P96$p\gamma/pp$ flux, in combination with a charm induced flux consistent with the TIG model. A better understanding of the charm production mechanism in the atmosphere will then be required to interpret such an observation of a small number of muons above the conventional atmospheric background.

This discussion has centred around a possible 'worst case' scenario (low AGN fluxes and uncertain charm fluxes). The larger fluxes considered in this work would be readily observable in a 20000 m^2 detector, using energy cuts of around 1-10 TeV. The planned deployments or extensions of the DUMAND, AMANDA, NESTOR and Lake Baikal experiments should herald the birth of observational extra-terrestrial neutrino astronomy, if the more optimistic AGN models and neutrino fluxes considered in this work are near to correct.

6 Acknowledgments

I thank F. Steffens, W. Melnitchouk, A. Thomas and G. Frichter for useful discussions on QCD and neutrino cross sections and R. Protheroe for clarifying aspects of AGN and atmospheric neutrino production. I thank B. Dawson and R. Clay for useful discussions, encouragement and careful reading of manuscripts and M. Roberts, T. Porter and J. Reid for their advice throughout the course of this work. An anonymous referee is also thanked for helpful comments on the original manuscript.

References

[1] F.W. Stecker, C. Done, M.H. Salamon, and P. Sommers. *Phys. Rev. Lett.* 66 (1991) 2697, Errata *Phys. Rev. Lett.* 69 (1992) 2738

[2] F.W. Stecker, C. Done, M.H. Salamon, and P. Sommers. *Proceedings of the Workshop on High Energy Neutrino Astronomy*, page 1. University of Hawaii, World Scientific, March 1992.

[3] F.W. Stecker and M.H. Salamon. *astro-ph/9501064 Space Science Reviews* (submitted) (1995)

[4] A.P. Szabo and R.J. Protheroe. *Proceedings of the Workshop on High Energy Neutrino Astronomy*, page 24. University of Hawaii, World Scientific, March 1992.

[5] A.P. Szabo and R.J. Protheroe. *Astropart. Phys.* 2 (1994) 365

[6] A. Roberts. *Rev. Mod. Phys.* 64 (1992) 259

[7] P.C. Mock et al. In *Proceedings of the 24th International Cosmic Ray Conference*, Rome, Italy, 1 (1995) 758

[8] I.A. Belolaptikov et al. In *Proceedings of the 24th International Cosmic Ray Conference*, Rome, Italy, 1 (1995) 742

[9] S. Bottai et al. In *Proceedings of the 24th International Cosmic Ray Conference*, Rome, Italy, 1 (1995) 1080

[10] T. Stanev. *Proceedings of the Workshop on High Energy Neutrino Astronomy*, page 354. University of Hawaii, World Scientific, March 1992.

[11] T. Stanev. *Nucl. Phys. B (Proc. Suppl.)* 35 (1994) 185

[12] V.J. Stenger. In *Proceedings of the Workshop: Trends in Astroparticle Physics*, Aachen, Germany, October 1991.

[13] E. Zas, F. Halzen and R.A. Vázquez *Astropart. Phys.* 1 (1993) 297

[14] T.K. Gaisser, F.Halzen, and T.Stanev. *Phys. Rep.* 258 (1995) 173

[15] G.M. Frichter, D.W. McKay, and J.P. Ralston. *Phys. Rev. D* 53 (1996) 1684

[16] R. Gandhi et al. *hep-ph/9512364 Astropart. Phys.* (submitted) (1995)

[17] R.J. Protheroe. In*Proceedings of the IAU Colloquium 163, Accretion Phenomena and Related Outflows,* edited by D. Wickramasinghe et al, 1996, in press

[18] A.D. Martin, W.J. Stirling, and R.G. Roberts. *Phys. Lett. B* 354 (1995) 155

[19] G.M. Frichter, D.W. McKay, and J.P. Ralston. *Phys. Rev. Lett.* 74 (1995) 1508

[20] I. Abt et al (H1 Collaboration) *Nucl. Phys. B* 407(1993) 515

[21] M. Derrick et al. (ZEUS Collaboration) *Phys. Lett. B* 316 (1993) 412

[22] T. Ahmed et al (H1 Collaboration) *Nucl. Phys. B* 439 (1995) 471

[23] M. Derrick et al (ZEUS Collaboration) *Z. Physik C - Part. and Fields* 65 (1995) 379

[24] P. Lipari. *Astropart. Phys.* 1 (1993) 195

[25] M. Thunman, G. Ingelman and P. Gondolo. *Nucl. Phys. B Proc. Suppl.* 43 (1995) 274

[26] H. Lai et al. *Phys. Rev. D* 51 (1995) 4763

[27] T.D. Lee. *Particle Physics and Introduction to Field Theory.* Harwood Academic, Switzerland, 1981.

[28] I.J.R. Aitchison and A.J. Hey. *Gauge Theories in Particle Physics: a Practical Introduction.* Adam Hilger, Bristol and Philadelphia, 2 edition, 1989.

[29] C.G. Callan and D.J. Gross. *Phys. Rev. Lett.* 22 (1969) 156

[30] T.K. Gaisser and A.F. Grillo. *Phys. Rev. D* 36 (1987) 2752

[31] Particle Data Group. Review of Particle Properties. *Phys. Rev. D* 50 (1994)

[32] J.G.H. de Groot et al. *Z. Physik C - Part. and Fields* 1 (1979) 143

[33] A.J. Buras. *Rev. Mod. Phys.* 52 (1980) 199

[34] M.H. Reno and C. Quigg. *Phys. Rev. D* 37 (1988) 657

[35] C. Quigg, M.H. Reno, and T.P. Walker. *Phys. Rev. Lett.* 57 (1986) 774

[36] M.H. Reno. *Proceedings of the Workshop on High Energy Neutrino Astronomy*, page 211. University of Hawaii, World Scientific, March 1992.

[37] V.N. Gribov and L.N. Lipatov. *Sov. J. Nucl. Phys.* 15 (1972) 675 *Yad. Fiz.* 15 (1972) 1218

[38] V.N. Gribov and L.N. Lipatov. *Sov. J. Nucl. Phys.* 15 (1972) 438 *Yad. Fiz.* 15 (1972) 781

[39] G. Altarelli and G. Parisi. *Nucl. Phys. B* 126 (1977) 298

[40] Y. L Dokshitser. *Sov. Phys. JETP* 46 (1977) 641 *Zh. Eksp. Teor. Fiz.* 73 (1977) 1216

[41] A.D. Martin, W.J. Stirling, and R.G. Roberts. *Phys. Rev. D* 47 (1993) 867

[42] A.D. Martin, W.J. Stirling, and R.G. Roberts. *Phys. Lett. B* 306 (1993) 145

[43] A.D. Martin, W.J.Stirling, and R.G.Roberts. *Phys. Rev. D* 50 (1994) 6734

[44] E.G. Floratos, C. Kounnas, and R Lacaze. *Nucl. Phys. B* 192 (1981) 417

[45] M. Glück, E. Reya, and A. Vogt. *Z. Physik C - Part. and Fields* 48 (1990) 471

[46] L.V. Gribov, E.M. Levin, and M.G. Ryskin. *Phys. Rep.* 100 (1983) 1

[47] T. Weigel and W. Melnitchouk. Submitted to *Nucl. Phys. B* (1995)

[48] M. Samorski and W. Stamm. *Ap. J.* 268 (1983) L17

[49] J. Lloyd-Evans et al. *Nature* 305 (1983) 784

[50] R.J. Protheroe, R.W. Clay, and P.R. Gerhardy. *Ap. J.* 280 (1984) L47

[51] G.B. Yodh. *Proceedings of the Workshop on High Energy Neutrino Astronomy*, page 257. University of Hawaii, World Scientific, March 1992.

[52] T.K. Gaisser and T. Stanev. *Phys. Rev. Lett.* 54 (1985) 2265

[53] T.K. Gaisser and T. Stanev. *Phys. Rev. D* 31 (1985) 2770

[54] E.W. Kolb, M.S. Turner, and T.P. Walker. *Phys. Rev. D* 32 (1985) 1145

[55] J.W. Cronin et al. *Phys. Rev. D* 45 (1992)

[56] A. Borione et al. In *Proceedings of the 24th International Cosmic Ray Conference*, Rome, Italy, 2 (1995) 439

[57] A. Borione et al. In *Proceedings of the 24th International Cosmic Ray Conference*, Rome, Italy, 2 (1995) 503

[58] A. Borione et al. In *Proceedings of the 24th International Cosmic Ray Conference*, Rome, Italy, 2 (1995) 430

[59] A. Borione et al. In *Proceedings of the 24th International Cosmic Ray Conference*, Rome, Italy, 2 (1995) 435

[60] T. Maccacaro et al. *Ap. J.* 374 (1991) 117

[61] K. Morisawa and F. Takahara. *Pub. Astron. Soc. Japan* 41 (1989) 873

[62] J. Chiang et al. *Ap. J.* 452 (1995) 156

[63] D.J. Thompson and C.E. Fichtel. *Astron. Astroph.* 109 (1982) 352

[64] J. Kwiecinski et al. *Phys. Rev. D* 42 (1990) 3645

[65] V.S. Berezinsky, A.Z. Gazizov, G.T. Zatsepin and I.L. Rozental. *Sov. J. Nucl. Phys.* 43 (1986) 406

[66] G.C. Hill. *PhD thesis, University of Adelaide* (1996)

[67] A.M. Dziewonski and D.L. Anderson. *Phys. Earth Planet. Inter.* 25 (1981) 297

[68] P. Lipari and T. Stanev. *Phys. Rev D* 44 (1991) 3543

[69] A.A. Petrukhin and V.V. Shestakov. *Can. J. Phys.* 46 (1968) S377 (10th ICRC Calgary).

[70] R.P. Kokoulin and A.A. Petrukhin. *Proceedings of the 12th International Cosmic Ray Conference (Hobart)*, 6 (1971) 2436

[71] L.B. Bezrukov and É.V. Bugaev. *Yad. Fiz.* 33 (1981) 1195 Sov. J. Nucl. Phys. 33 (1981)

[72] V.J. Stenger. *Proceedings of the 1992 NESTOR Workshop, Pylos, Greece*, 1992.

[73] W. Rhode et al. *Astropart. Phys.* (submitted) (1995)

[74] W. Rhode et al. In *Proceedings of the 24th International Cosmic Ray Conference*, Rome, Italy, 1 (1995) 781

[75] T.K. Gaisser. *Nucl. Phys. B (Proc. Suppl.)* 31 (1993) 399